Arrays of weakly coupled, periodically poled lithium niobate waveguides: beam propagation and discrete spatial quadratic solitons

R. IWANOW[*1], R. SCHIEK[1], G. STEGEMAN[1], T. PERTSCH[2], F. LEDERER[2], Y. MIN[3], and W. SOHLER[3]

[1]College of Optics and Photonics, FPCE and CREOL, University of Central Florida, Orlando, USA
[2]Friedrich-Schiller University, Jena, Germany
[3]University of Paderborn, Paderborn, Germany

Discrete optical systems can be realized as arrays of parallel, weakly coupled, channel waveguides where light normally undergoes "discrete diffraction" via the weak coupling between adjacent channels. Here we describe how light can be forced to maintain a constant field profile on propagation in waveguide arrays, i.e., to localize into a discrete spatial soliton, by using the second order nonlinearity of periodically poled lithium niobate near phase-matching for second harmonic generation. Detailed sample characterization and experimental verification of the excitation of discrete quadratic solitons is reported.

Keywords: solitons, nonlinear optics, integrated optics.

1. Introduction

When two parallel, identical two-dimensional waveguides are placed in sufficiently close proximity that their modes overlap, light can be coupled from one waveguide to the other via tunnelling across the gap between the guides [1,2]. There is a $\pi/2$ phase shift associated with the coupling as the energy is transferred to the adjacent channel. This device is known in integrated optics as a dual directional coupler. When the device length is terminated exactly at the linear coupling length, light is completely switched from the input to the adjacent channel. This switching can be prevented by detuning the optical properties (propagation constants or effective indices) of the two waveguides. This can be achieved either electro-optically, or all-optically [3,4]. The simplest example of all-optical detuning is to utilize a Kerr nonlinearity and detune the input channel by applying high enough intensities to significantly change the local refractive index.

If the input channel is embedded within an array of channels the light can be coupled to two adjacent channels corresponding to a form of discrete diffraction [2,5,6]. In this way light can spread throughout the array. Now the $\pi/2$ phase shift plays a critical role in the way light spreads in the array. In the extreme case of excitation of only one channel, the pattern exhibits two well-defined power lobes travelling at equal angles out from the excitation channel, leaving only small intensities in the input and its adjacent channels. In the other limit, for wide excitation beams overlapping many channels, the diffraction pattern resembles closely that associated with diffraction in continuous media, i.e., the intensity maximum tracks the central channel. If the channels of the array exhibit a self-focusing Kerr nonlinearity, energy transfer between channels can be again arrested at high input intensities, just like in the directional coupler case, and the beam is localized to its input channels as it propagates down the waveguide [7]. This corresponds to a discrete Kerr soliton which has been reported in the literature [8]. It is the continuous medium analogue of a 1D spatial Kerr soliton in a slab waveguide [9].

It is now well-known that a cascading induced nonlinear phase shift which occurs near phase-matching for second harmonic generation (SHG) can also lead to a self-focusing of both the fundamental and harmonic beams [10]. In fact, the transfer between the two channels of a dual directional coupler has been inhibited at high intensities solely due to this cascaded $\chi^{(2)}$-effect [11]. Furthermore, mutually self-trapped fundamental and harmonic beams, i.e., spatial solitons, have been observed in 1D (slab waveguides) and 2D (bulk media) due to their interaction via the second order nonlinearity [12,13]. Thus, it is not surprising that discrete "quadratic" solitons have been predicted theoretically to exist in weakly coupled arrays of channel waveguides tuned close to phase-matching for SHG [14–16].

This paper describes the observation of discrete quadratic solitons in periodically poled lithium niobate waveguide arrays. A brief initial report has already published in letter format and this paper is meant to give a detailed discussion of the samples, their characterization, the apparatus used in the experiments and the observations [17].

*e-mail: riwanow@mail.ucf.edu

2. Periodically poled lithium niobate arrays and their characterization

The 7-cm long, Z-cut LiNbO$_3$ samples were cut along the X-axis from 4 inch congruent wafers. The channel waveguides were fabricated by Ti-indiffusion. Electric field assisted periodic poling was used to create a quasi--phase-matched (QPM) structure [18]. It was necessary to address a number of key issues in order to achieve the required waveguide quality and reproducibility, and these were thoroughly investigated. In order to achieve a high degree of homogeneity, uniformity of Ti-deposition, photolithographic Ti-stripe definition, Ti-indiffusion and periodic poling were optimised. In particular, for electric field assisted periodic poling, various parameters such as a temperature, poling voltage, poling current, total charge and voltage profile were precisely controlled to get a homogeneous microdomain structure with the optimum duty cycle of 1:1. As a result, a variety of Ti:PPLN waveguide structures of excellent properties could be developed.

The procedure steps, developed over 20 years at the University of Paderborn, are summarized in Fig. 1. The arrays, four to a sample each containing 101 channels were fabricated over the full 7-cm length of the samples. The spacing between individual channels was different in each array, varying from 14 to 16 μm, in order to allow different coupling lengths between adjacent channels. Isolated single "witness" channels, in which linear losses and SHG efficiency could be measured, were placed between each set of arrays. Representative micrographs of the end-face (in-coupling facet) of a sample, and also taken from above after selective etching to make visible both the individual channel as well as the periodically poled regions, are shown in Fig. 2. Based on the fabrication parameters, the index distribution within the material due to Ti-indiffusion was modelled, and the modal field distributions at both the fundamental (FW at 1560 nm) and second harmonic (SH at 780 nm) fields were calculated numerically with excellent agreement with the measured mode profiles and are shown in Fig. 3 [19]. Note that although the field distributions of adjacent channels overlap for the FW, the overlap is essentially zero for the SH.

The fabrication of arrays with 101 channels that are identical over 7 cm was technologically challenging. The
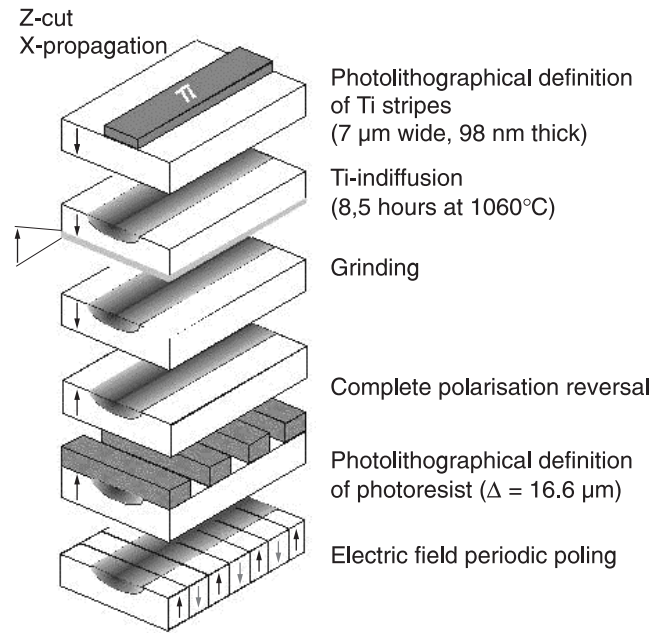

Fig. 1. Schematical representation of the steps for Ti:PPLN channel waveguide fabrication.

uniformity of each array was evaluated by injecting light at 1560 nm into single channels and then measuring the intensity distribution at the output. This allowed regions in arrays without channel breaks, inhomogeneities and scattering sites due to imperfect poling etc. to be identified. Assuming that coupling only occurs between nearest neighbours, the equation describing the evolution of the field amplitude a_n in the centre of the n-th channel is given by

$$-i\frac{da_n}{dx} + \beta a_n + c(a_{n+1} + a_{n-1}) = 0, \qquad (1)$$

where $c = \pi/2L_c$ is the coupling constant, L_c is the half--beat coupling length, x is the propagation direction, and β is the propagation constant (wavevector) for an isolated individual channel [5]. Thus, light spreads throughout the array via nearest neighbour coupling. It has been shown that the field distribution at the output facet when only the $n = 0$ channel is excited is given by

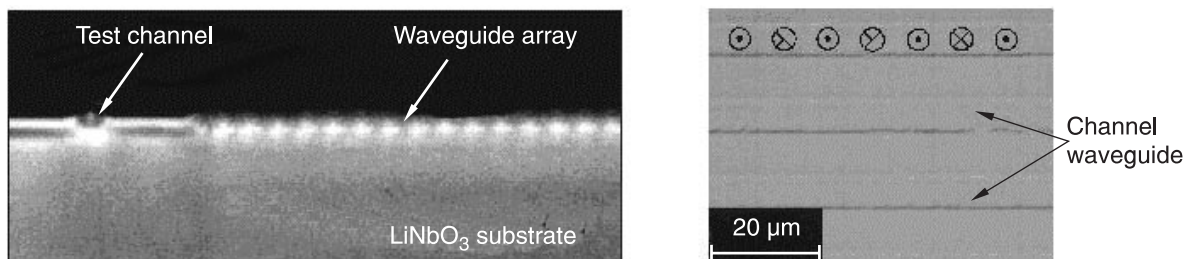$$E_n(x) = (-i)^n J_n(2cx), \qquad (2)$$

Fig. 2. Microphotographs of the polished end face of a part of a waveguide array illuminated from the input side (left), and of the periodically poled microdomain structure of a waveguide array observed from above after preferential etching (right). The periodic orientation of the Z-axis is indicated.
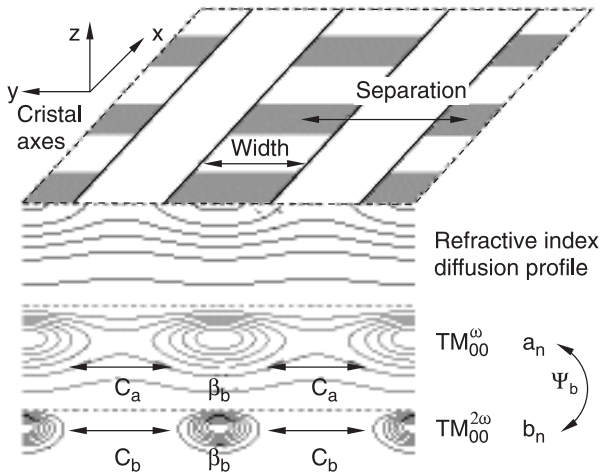
Fig. 3. Typical refractive index distribution and the fundamental and harmonic mode profiles for Z-cut, X-propagation Ti:PPLN channel waveguides in a periodic array.

Fig. 5. SHG detuning curves for two witness channels.

where J_n is the n-th order Bessel function. An example of a measured discrete diffraction pattern is shown in Fig. 4, as well as the best fit used to evaluate the coupling length L_c which was found to be 15.7 mm in this case. The fit between experiment and theory is excellent, indicating an excellent quality region of the array. Note the characteristic of single channel excitation with strong side-lobes into which most of the energy flows.

Linear and nonlinear characterization of the appropriate "witness" channels was performed once the suitable array for the soliton experiment was identified. The losses were measured to be ~0.15 dB/cm and ~0.30 dB/cm at the FW and SH wavelengths respectively. The SH tuning curves were also measured for the witness channels, at the temperature of 195°C and they are shown in Fig. 5. Note that it was necessary to investigate the sample in an oven in order
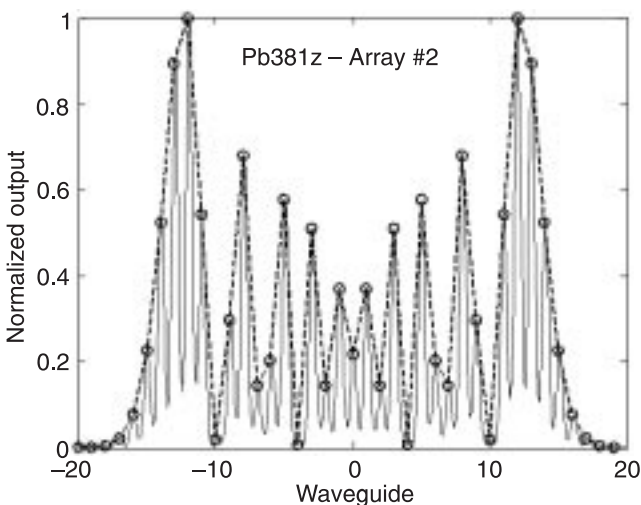
to minimize photorefractive effect which was observed at temperatures below 150°C. The oven introduced temperature gradients near the end faces of the samples. The measured distortions of the detuning curves away from the classical $sinc^2$ response are a combined result of the temperature gradient at the sample ends and width variation of individual channels – both influencing the local wavevector mismatch.

3. Linear wave propagation in arrays

The coupling between adjacent channels not only leads to "discrete diffraction" but also to the propagation of beams across the array [6]. The dispersion relation for "plane waves" is obtained by exciting each channel with the equal amplitude a_0 and with a relative phase between channels of $\Delta\phi$. The Bloch wavevector k_y associated with the periodic structure can be defined by $k_y = \Delta\phi/d$ where d is the centre-to-centre channel spacing. Assuming "plane wave" solutions of the form

$$a_n = E_0 \exp[i\{\omega t - k_x x - n k_y d\}], \qquad (3)$$

and substituting into Eq. (1) gives the dispersion relation

$$k_x = \beta + 2c \cos[k_y d]. \qquad (4)$$

This dispersion relation is plotted in Fig. 6.

There are two immediate repercussions to such a periodic dispersion relation. The spatial diffraction coefficient is given by

$$D = \frac{d^2 k_x}{dk_y^2}, \qquad D = -2cd^2 \cos(k_y d). \qquad (5)$$

Fig. 4. Measured "discrete diffraction" pattern (solid line) at the output for single channel excitation. The best fit to the theoretical [Eq. (2)] diffraction pattern (at the centres of the channels) is given by the circles. The dashed lines are guides to the eye.
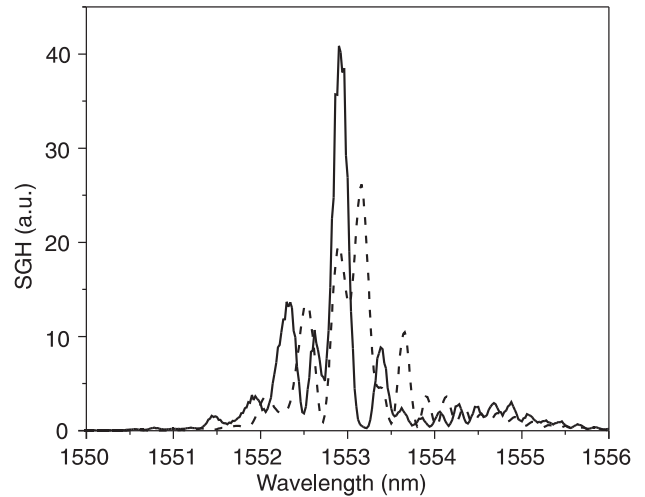
This result predicts that maximum beam broadening occurs for $k_y d = \pm n\pi$ for $n = 0, 1, 2,...$ where-as for $k_y d = \pm(n + 1/2)\pi$ the diffraction is zero, i.e., there is no beam spreading. This was verified experimentally [20] in the LiNbO$_3$
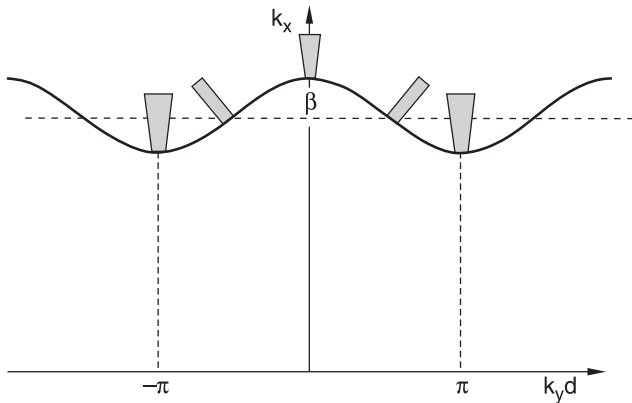
Fig. 6. Theoretical propagation vector dispersion relation for a discrete system. Beam diffracts with maximum strength at $k_y d = \pm n\pi$. There is no diffraction at $k_y d = \pm(n + 1/2)\pi$.

Fig. 8. Output power distribution vs. relative phase difference between adjacent channels for a 4-channel wide input beam.

with results shown in Fig. 7. Note that at $k_y d = \pm\pi/2$ there is no increase in the width of the beam transmitted through the array. Furthermore, depending on the relative input phase between adjacent channels, the beam slides across the array. The displacement of the beam's centre channel at the output facet relative to the beam centre's input channel should vary proportional to $\sin(k_y d)$, i.e., it should be a maximum at $k_y d = \pm\pi/2$, and zero at $k_y d = \pm n\pi$. The actual measurements, shown in Fig. 8, agree with these predictions. Note that there the maximum propagation angle across the array relative to the x-axis for weak coupling is given by $\pm\pi/2\beta d$.

All of the measurements discussed above were taken for propagation of the FW beam at ~1560 nm, i.e., at low powers so that essentially no SH is generated. At high input powers, SH is generated. Because the coupling coefficient for the SH is very small, as illustrated by the modal profiles in Fig. 3, there is effectively no coupling between the SH fields in the individual channels. However, SH does appear

in neighbouring channels due to generation from the FW present in that channel. This is shown schematically in Fig. 9. Mathematically, there is no dispersion in the SH wavevector $k_z = \beta(2\omega)$ with input phase angle between adjacent channels.

4. Discrete quadratic solitons: theory

The introduction of the second order nonlinearity which couples the FW to the SH waves, and which is known to lead to effective self-focusing and self-defocusing nonlinearities can lead to solitons. As mentioned previously, this has led to the observation of quadratic solitons in 1D (slab waveguide) and 2D (bulk) media. Similarly for the discrete case, including this coupling has been predicted to lead to discrete quadratic solitons in 1D (and probably also in 2D) [14–16].

The relevant discrete equations now become

$$
\begin{aligned}
i\frac{\partial a_n}{\partial x} + c(a_{n+1} + a_{n-1}) &= -\omega\gamma a_n^* b_n \exp[-i\Delta\beta x] \\
i\frac{\partial b_n}{\partial x} &= -\omega\gamma a_n^2 \exp[i\Delta\beta x]
\end{aligned}
, \quad (6)
$$

where a_n and b_n are the FW and SH field amplitudes in the channel, $\gamma = (\varepsilon_0/2)(\chi_{eff}^{(2)}/2)K$ where K is a mode overlap
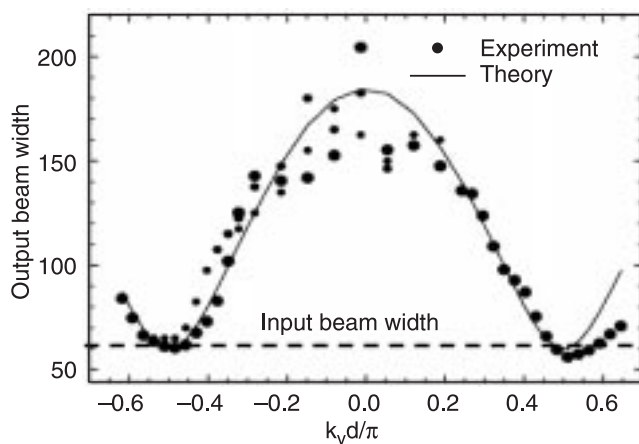

Fig. 7. Experimental results on linear beam propagation in the Ti:PPLN waveguide arrays. Notice that for the relative phase difference between adjacent channels of $k_y d = \pm\pi/2$ diffraction vanishes when the output beam width equals the input beam width of 60 μm.
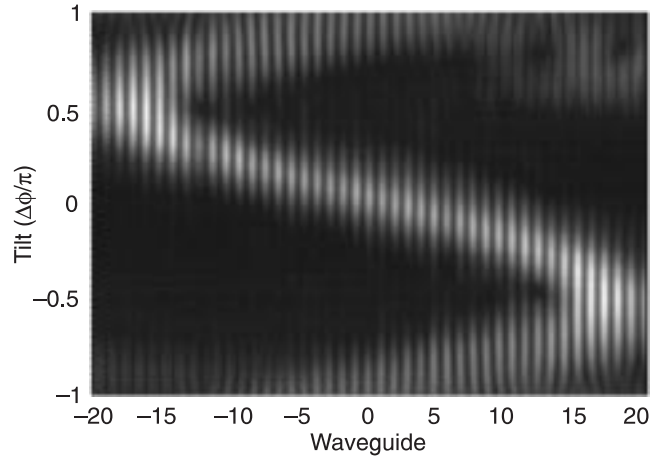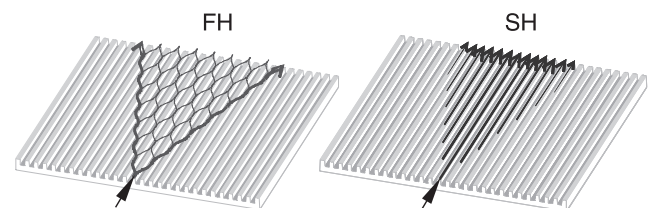

Fig. 9. Schematic representation of the discrete diffraction at the fundamental wavelength (left-hand-side), and the lack of discrete diffraction for the harmonic which is generated independently in each channel by the fundamental present.
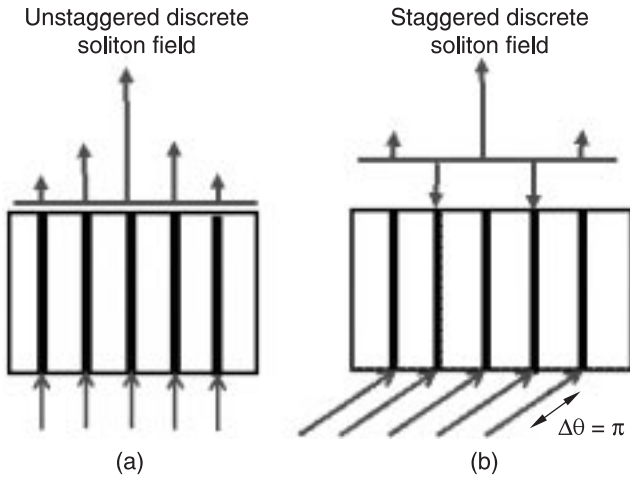
Fig. 10. Stable "unstaggered" and "staggered" discrete soliton fundamental field distributions at the center of each channel and their excitation conditions in the array.

integral and $\Delta\beta = 2k_x - \beta(2\omega) \pm 2\pi/\Lambda$ where $\beta(2\omega)$ is the guided wave wavevector at the harmonic frequency and Λ is the QPM period. Because the inter-channel coupling between the harmonic fields is very small, it has been neglected, as discussed previously with regard to Fig. 3. Note that in the previous theoretical work it was assumed that the coupling constant for the SH field was comparable to that for the FW field.

There are four solutions to Eq. (6) for bright solitons whose energy propagates along the *x*-axis without spreading [14–16]. They depend on the sign of the nonlinearity, self-focusing for $\Delta\beta > 0$ or self-defocusing for $\Delta\beta < 0$, and the sign of the diffraction coefficient *D*, negative for normal diffraction and positive for anomalous diffraction. The field "symmetry" is either "unstaggered" with all of the fields in adjacent channels in phase, or "staggered" in which the fields in adjacent channels are π out-of-phase with one another. These are illustrated in Fig. 10. The former occurs for $\Delta\beta > 0$ and *D* negative, and the latter for $\Delta\beta < 0$ and *D* positive. In addition, the peak amplitudes can lie either on a channel (shown in Fig. 10) or between channels

(not shown in Fig. 10). Only the "on channel" case is stable and small perturbations cause this case to evolve into the stable one.

The "wrong" combination of signs for the diffraction coefficient and nonlinearity leads to enhanced diffraction. This would occur for *D* negative and $\Delta\beta < 0$, as well as for *D* positive and $\Delta\beta > 0$.

5. Experimental setup

The properties of the laser source required were set by the power required for discrete soliton excitation, the sample length (which determines the SHG and therefore laser bandwidth) and the temporal walk-off between FW and SH due to their different group velocities. For the 7-cm long samples at 1560 nm, an ideal source bandwidth should be less than 0.2 nm which corresponds to a pulse length of 12 ps for a bandwidth limited pulse.

Furthermore, theoretical calculations show that the minimum power required for soliton excitation on SHG phase-match is of the order of a few 100 Watts [14–16]. Off phase-match, the required power scales approximately linearly with the phase-mismatch. Given the losses in a typical optical system for shaping and characterizing the input beam, at least an additional factor of two more in power is needed. Our target was 5 kW.

Secondary but still important requirements were the pulse-to-pulse stability and the source's repetition rate. The first relates to the reproducibility of the results and the second to the signal-to-noise ratio of power measured by detectors. These parameters were set at a minimum of 1 MHz for the repetition rate and pulse-to-pulse stability better than 5%.

The source laser was a Pritel FFL-1000 Er-doped fiber laser which produced transform limited pulses over the wavelength range 1535–1565 nm at a 5-MHz repetition rate. It was necessary for the experiments to amplify the pulses in a fiber amplifier to an output of 5 kW of peak power with minimal self-phase modulation. A dual core power fiber amplifier from KEOPSYS was used. It was necessary to use a pulse stretcher before the amplifier to re-
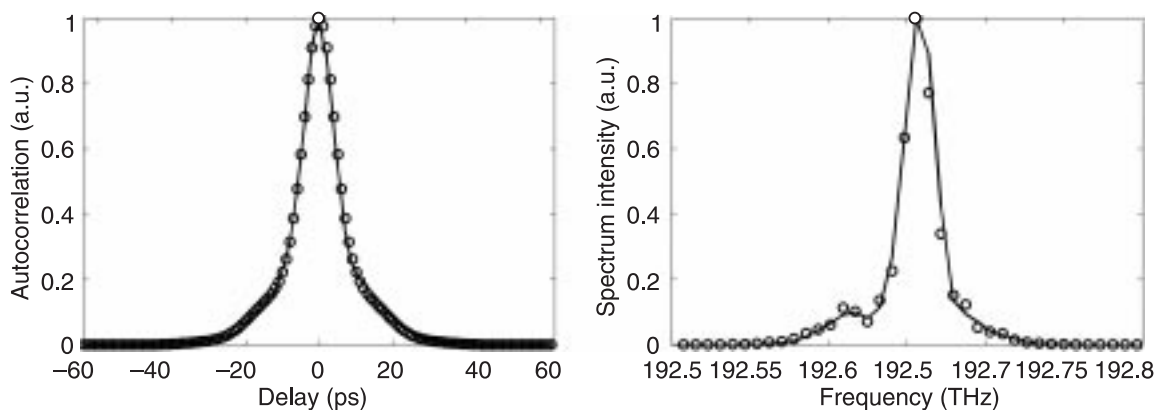

Fig. 11 Temporal autocorrelation (left) and spectral intensity (right): circles – experiment, solid line – calculated from the FROG retrieved pulse.
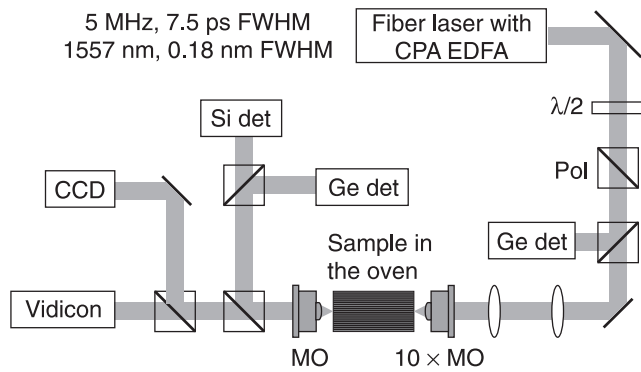
Fig. 12. Experimental setup.

Fig. 13. Fundamental wavelength output energy distribution vs. total input peak power for the "unstaggered" case.

duce the peak intensity (and hence the spectral broadening due to self-phase modulation). A custom-made chirped fiber grating was obtained from Ian Bennion's group at Aston University in the UK. It is the spectral response of this grating which limited the tuning range of the amplifier system to 8 nm. The amplified pulses were then recompressed in a bulk grating compressor operated at near grazing incidence.

The output from the compressor (available for the experiments) was measured with both an autocorrelator and a FROG system, and the results are shown in Fig. 11. The pulse width was measured to be 7.7 ps and the spectral bandwidth was 0.22 nm, FWHM and the peak power exceeding 4 kW.

The layout of the total experimental system is shown in Fig. 12. Germanium detectors and cameras were used to measure the incident, transmitted pulse energies and the output beam profiles respectively. Silicon detectors and cameras were used to measure the output harmonic component. Combinations of spherical and cylindrical lenses were used to shape the beam into an elliptical cross-section with a planar phase-front at the input facet of the sample. The sample was held in an adjustable mount with multiple degrees of translational and rotational freedom to facilitate both coarse and fine adjustments of the sample relative to the input beam.

6. Experiments on nonlinear beam propagation

The first set of experiments dealt with a demonstration of "unstaggered" solitons, i.e., the channels were all excited with the same phase. The incident FW beam was adjusted to give a FWHM of 62 μm, which corresponds to an excitation of about 4–4.5 channels. The intensity maximum was adjusted laterally until it coincided with a channel. The SH associated with the solitons is generated with distance into the individual channels, a common practice for exciting quadratic soliton [21].

The results obtained by ramping the input power and measuring the output intensity profile from the array are shown in Fig. 13. The collapse of the output beam with increasing power is clear, leading to the formation of a discrete quadratic soliton by 300 W peak power in the com-
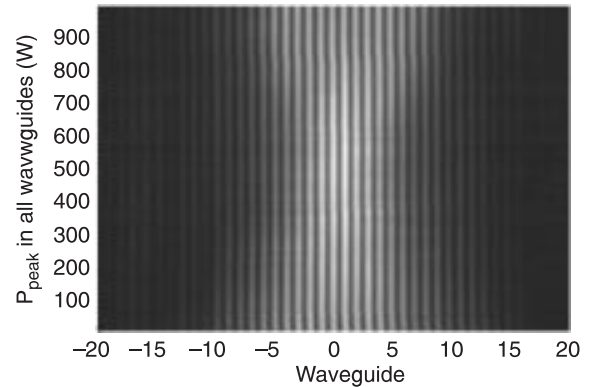
bined waveguides. As power is increased further, solitons are excited up to about 650 W peak power. A corresponding output intensity profile is shown in Fig. 14 at a peak power of 530 W. Shown there are the linearly (low power) diffracted beam profile, the theoretically calculated diffraction profile and both – experimental and calculated soliton profiles. The agreement is excellent. Further increases in power led to a broadening of the output beam profile due to combined effects of multiphoton absorption [22], green induced infrared absorption [23] and photorefractivity which "flattens" the peak of the profile.

The generation of "staggered" beams in the waveguide array was facilitated by tilting the input beam until the relative phase between adjacent channels was π. Shown in Figs. 15 and 16 are respectively, the power evolution at the output facet and the detailed intensity output profile in the power range in which a staggered soliton is excited. The power evolution plot again indicates a collapse of the output beam into a soliton at the output, this time requiring 140 W peak power in all of the channels. The agreement between the intensity profiles for the experimental and calculated soliton shapes is in excellent agreement, although the agreement between the theoretical and calculated diffraction patterns is not as good. This is a consequence of
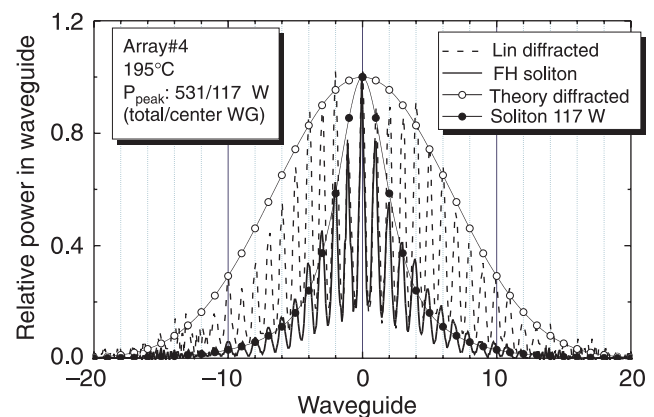

Fig. 14. Comparison of experimental and calculated output energy distributions for the diffracted beam and the soliton for the "unstaggered" case.
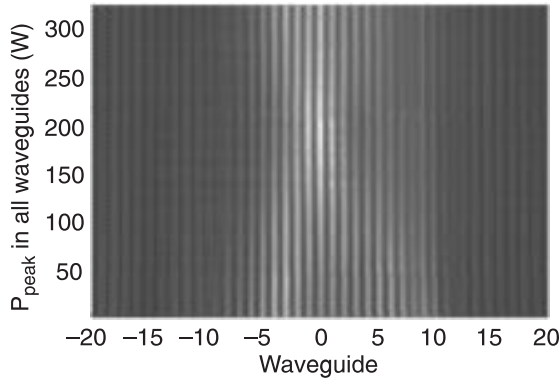
Fig. 15. Fundamental wavelength output energy distribution vs. total input peak power for the "staggered" case.

Fig. 17. Dependence of the threshold power required for soliton formation vs. wavevector mismatch for samples with different coupling lengths.

the excitation method used which puts power into higher order Floquet-Bloch bands of the periodic structure when operating at the edge of the first Brillouin zone (which corresponds to the π phase shift between channels) [24].

By tuning the temperature of the sample it is possible to not only operate on both sides of phase matching, but also to change the phase-mismatch systematically. It is known that the magnitude of the cascading nonlinearity increases when tuning the wavevector mismatch closer to the phase-match condition. Furthermore, the power required to excite discrete quadratic solitons is expected to decrease as the coupling length increases (and the coupling coefficient c decreases). All of these features characteristic of $\chi^{(2)}$-mediated discrete solitons were tested and the results are shown in Fig. 17. Indeed the peak power required for soliton formation was found to decrease with decreasing wavevector mismatch, both from the positive and negative detuning sides. Furthermore, the power required also decreases with coupling coefficient decrease. These results verify that indeed these are quadratic solitons.
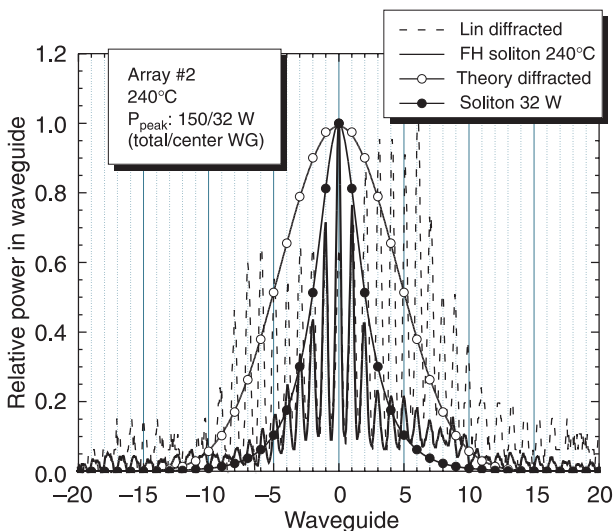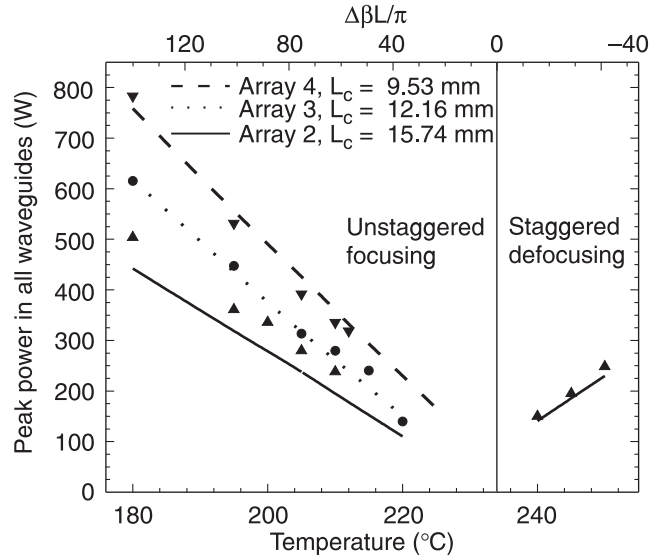
Two additional sets of experiments were performed for conditions under which no solitons are expected to exist. An "unstaggered" beam was directed onto the input facet for $\Delta\beta < 0$. It is expected theoretically, as discussed above, that in this case increasing power will lead to an enhanced (wider) diffraction pattern. This was indeed observed experimentally. An example of the increased width of the intensity profile is shown in Fig. 18.

Finally, the stability of the solutions to the nonlinear generating Eq. 6 was checked experimentally with the results shown in Fig. 19. When the input beam was centred between channels, noise on the beams is sufficient to cause the output beam centre to move back and forth between the two adjacent channels. On the other hand, when the input beam is centred on one channel, the output is stable. This verifies that stable solitons exist only for beams centred on a channel.

Fig. 16. Comparison of experimental and calculated output energy distributions for both the diffracted beam and soliton for the "staggered" case.
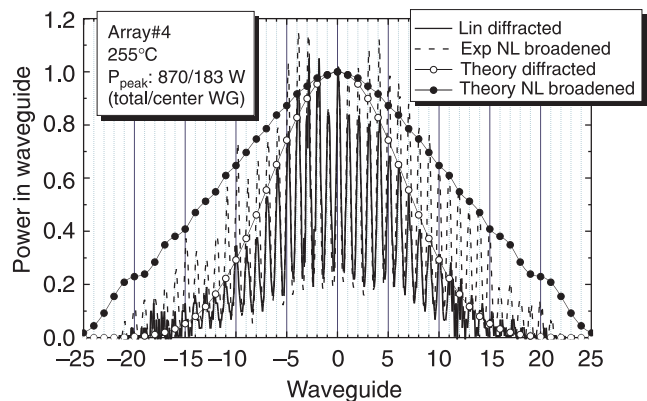

Fig. 18. Comparison of experimental and calculated output energy distributions for a linearly diffracted beam and a nonlinearly broadened beam for the "unstaggered case" $\Delta\beta < 0$ and $D < 0$.
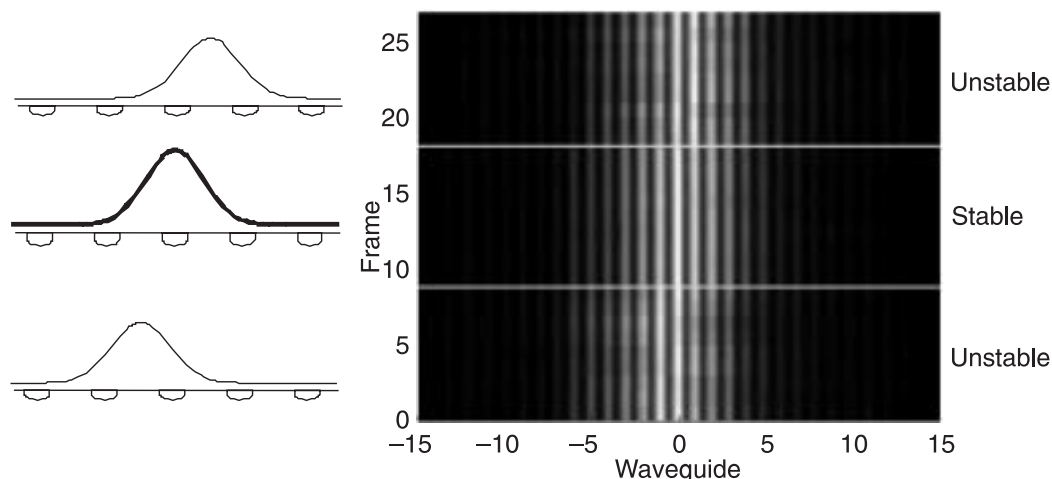
Fig. 19. Output intensity distribution as a function of time for three different positions of the input beam relative to the central channels.

7. Conclusions

We have defined the conditions under which discrete quadratic solitons could be observed in PPLN arrays. Arrays of 101 Ti-indiffused waveguides were fabricated and prepared for phase-matching SHG at 1560 nm by periodic poling. The waveguides were characterized for losses, SHG efficiency, and their discrete diffraction patterns.

A laser system and experimental apparatus was built with the appropriate characteristics for exciting discrete quadratic solitons in these arrays. At FW power levels of 100 W, discrete solitons of both the "unstaggered" and "staggered" variety were observed experimentally. Additional measurements as a function of phase-mismatch established that the solitons observed really were due to the second order nonlinearity.

References

1. E.A. Marcatili, "Dielectric rectangular waveguide and directional coupler for integrated optics", *At.&T. Tech. J.* **48**, 2071 (1969).
2. S. Somekh, E. Garmire, A. Yariv, H.L. Garvin, and R. G. Hunsperg, "Channel optical waveguide directional couplers", *Appl. Phys. Lett.* **22**, 46–47 (1973).
3. M. Papuchon, Y. Combemale, X. Mathieu, D.B. Ostrowsky, L. Reiber, A.M. Roy, B. Sejourne, and M. Werner, "Electrically switched optical directional coupler – cobra", *Appl. Phys. Lett.* **27**, 289–291 (1975).
4. S.R. Friberg, Y. Silberberg, M.K. Oliver, M.J. Andrejco, M.A. Saifi, and P.W. Smith, "Ultrafast all-optical switching in a dual-core fiber nonlinear coupler", *Appl. Phys. Lett.* **51**, 1135–1137 (1987).
5. A.L. Jones, "Coupling of optical fibers and scattering in fibers", *J. Opt. Soc. Am.* **55**, 261 (1965).
6. D.N. Christodoulides, F. Lederer, and Y. Silberberg, "Discretizing light behaviour in linear and nonlinear waveguide lattices", *Nature* **424**, 817–823 (2003).
7. D.N. Christodoulides and R.I. Joseph, "Discrete self-focusing in nonlinear arrays of coupled wave-guides", *Opt. Lett.* **13**, 794–796 (1988).
8. H.S. Eisenberg, Y. Silberberg, R. Morandotti, A.R. Boyd, and J.S. Aitchison, "Discrete spatial optical solitons in waveguide arrays", *Phys. Rev. Lett.* **81**, 3383–3386 (1998).
9. J. S. Aitchison, A.M. Weiner, Y. Silberberg, M.K. Oliver, J.L. Jackel, D.E. Leaird, E.M. Vogel, and P.W.E. Smith, "Observation of spatial optical solitons in a nonlinear glass wave-guide", *Opt. Lett.* **15**, 471–473 (1990).
10. G.I. Stegeman, D.J. Hagan, and L. Torner, "$\chi^{(2)}$ cascading phenomena and their applications to all-optical signal processing, mode-locking, pulse compression and solitons", *Opt. Quant. Electron.* **28**, 1691–1740 (1996).
11. R. Schiek, Y. Baek, G. Krijnen, G.I. Stegeman, I. Baumann, and W. Sohler, "All-optical switching in lithium niobate directional couplers with cascaded nonlinearity", *Opt. Lett.* **21**, 940–942 (1996).
12. R. Schiek, Y. Baek, and G.I. Stegeman, "One-dimensional spatial solitary waves due to cascaded second-order nonlinearities in planar waveguides", *Phys. Rev.* **E53**, 1138–1141 (1996).
13. W.E. Torruellas, Z. Wang, D.J. Hagan, E.W. Van Stryland, G.I. Stegeman, L. Torner, and C.R. Menyuk, "Observation of 2-dimensional spatial solitary waves in a quadratic edium", *Phys. Rev. Lett.* **74**, 5036–5039 (1995).
14. S. Darmanyan, A. Kobyakov, and F. Lederer, "Strongly localized modes in discrete systems with quadratic nonlinearity", *Phys. Rev.* **E57**, 2344–2349 (1998).
15. T. Peschel, U. Peschel, and F. Lederer, "Discrete bright solitary waves in quadratically nonlinear media", *Phys. Rev.* **E57**, 1127–1133 (1998).
16. C. Etrich, F. Lederer, B. Malomed, T. Peschel, and U. Peschel, "Optical solitons in media with a quadratic nonlinearity", in *Progress in Optics*, edited by Elsevier (2000).
17. R. Iwanow, R. Schiek, G.I. Stegeman, T. Pertsch, F. Lederer, Y. Min, and W. Sohler, "Observation of discrete quadratic solitons", *Phys. Rev. Lett.* **93**, 113902 (2004).

18. D. Hofmann, G. Schreiber, C. Haase, H. Herrmann, W. Grundkotter, R. Ricken, and W. Sohler, "Quasi-phase-matched difference-frequency generation in periodically poled Ti : LiNbO₃ channel waveguides", *Opt. Lett.* **24**, 896–898 (1999).

19. E. Strake, G.P. Bava, and I. Montrosset, "Guided modes of Ti-LiNbO₃ channel wave-guides – a novel quasi-analytical technique in comparison with the scalar finite-element method", *J. Lightwave Technol.* **6**, 1126–1135 (1988).

20. R. Iwanow, R. Schiek, G.I. Stegeman, T. Pertsch, F. Lederer, Y. Min, and W. Sohler, "Diffractionless propagation in low loss LiNbO₃ channel waveguide arrays", *CLEO*, CTuK13 (2002).

21. A.V. Buryak, P. Di Trapani, D.V. Skryabin, and S. Trillo, "Optical solitons due to quadratic nonlinearities: from basic physics to futuristic applications", *Phys. Rep.* **370**, 63–235 (2002).

22. D. von der Linde, A.M. Glass, and K.F. Rodgers, "Multiphoton photorefractive processes for optical storage in LiNbO₃", *Appl. Phys. Lett.* **25**, 155–157 (1974).

23. Y. Furukawa, K. Kitamura, A. Alexandrovski, R.K. Route, M.M. Fejer, and G. Foulon, "Green-induced infrared absorption in MgO doped LiNbO₃", *Appl. Phys. Lett.* **78**, 1970–1972 (2001).

24. D. Mandelik, H.S. Eisenberg, Y. Silberberg, R. Morandotti, and J.S. Aitchison, "Band-gap structure of waveguide arrays and excitation of Floquet-Bloch solitons", *Phys. Rev. Lett.* **90**, 053902 (2003).

MIOMD-VII
Mid Infrared Optoelectronics: Materials and Devices

12th –14th September 2005, Lancaster University, UK

Second Call for Papers

The Scientific Committee invite the submission of abstracts on topics of interest to the mid-infrared community including, but not limited to:

Injection lasers	Quantum cascade lasers
Photodetectors	QWIPs and QDIPs
MIR applications	TDLS
LEDs & NL devices	Materials growth and characterisation

Confirmed Invited Speakers

F. Capasso *(Harvard University)*	J. Meyer *(USN, Washington)*
S. Krishna *(University of New Mexico)*	K.D. Moiseev *(Ioffe Institute, St Petersburg)*
Aizhen Li *(IMT, Shanghai)*	B. Jean *(University Hospital Tübingen)*
A. Baranov *(University of Montpellier)*	M-C Amann *(Walter Schottky Institute)*
J. Cockburn *(University of Sheffield)*	A. Garnache *(University of Montpellier)*
M. Rattunde *(Fraunhofer IAF)*	G. Springholz *(University of Linz)*
M. Razeghi *(Northwestern University)*	V. A. Solov'ev *(Ioffe Institute, St Petersburg)*

Abstract submission deadline: 7th May 2005
Registration deadline: 15th July 2005

http://www.lancs.ac.uk/depts/physics/conf/miomd-7/index.htm